A new method for locating and quantifying damage in beams from static deflection changes

N.T. Le[a,*], D.P. Thambiratnam[a], A. Nguyen[b], T.H.T Chan[a]

[a] *Queensland University of Technology, Australia,* [*] *Email:* ngocthach.le@hdr.qut.edu.au
[b] *University of Southern Queensland, Australia*

Abstract

This paper presents a new method that can locate and quantify damage in Euler-Bernoulli beams from changes in static deflection. Using the principle of Virtual Work, for the first time, the deflection change (*DC*) parameter is formulated as a function of both the damage location and damage severity. Through this, the study shows that the changes in static deflection follow certain patterns that clearly reveal the damage location. Therefore, by observing a plot of the measured *DC*, the damage locations can be identified conveniently. Once the damage is located, its severity is estimated directly from the measured relative deflection change through a new concept named damage severity consistency (*DSC*) function. A constant or nearly constant *DSC* function indicates a high precision of the damage detection results and reflects a good quality of the measurement data. Numerical and laboratory investigations demonstrate that the method accurately locates and quantifies the damage under various scenarios in statically determinate beams. The proposed damage detection method has a clear theoretical base, does not rely on an optimization algorithm, and can be extended to other beam-type structures including statically indeterminate beams.

Keywords: Structural health monitoring, static damage detection, static deflection, static relative deflection, damage locating, damage quantification, structural damage

1. Introduction

Unexpected changes in operational conditions can cause cumulative damage in civil structures such as buildings, bridges and dams. If an initial damage in these structures is not detected timely, it can lead to increased damage and even catastrophic failure. The need to monitor structural performance and detect the onset of damage are thus evident. Structural Health Monitoring (SHM) has emerged as a feasible technique for this purpose by using on-structure, non-destructive sensing systems [1]. Within the SHM context, damage can be defined as changes introduced into a system (cracks, corrosions, bolt loosening, etc.), either intentional or unintentional, which adversely affect the current or future performance of that system [2]. Over the past few decades, the research on damage detection (DD) methods has received considerable attention. The fundamental idea of the methods is that damage in a structure, when significant enough, can cause detectable changes in the structural responses. Therefore, by measuring these changes, one can assess the damage with respect to its presence, location and severity. The effects of damage on a structure can be classified as linear or nonlinear. A linear damage situation is defined as the case when the initially linear-elastic structure remains linear-elastic after damage [2]. As evidenced from the literature, this assumption has been widely used in the majority of current DD methods.

The existing DD methods can also be classified into three major categories, i.e., the dynamic DD methods using measured vibration characteristics, the static DD methods using static measurement data, and the static-dynamic DD methods utilising both static and dynamic parameters. The dynamic DD techniques have been more fully developed compared to the static counterpart, and the corresponding literature is quite extensive as evidenced from the reviews of Doebling *et al.* [2], Sohn *et al.* [3], and Fan and Qiao [4]. Although many dynamic DD methods have shown to be promising, there are still a number of inherent difficulties that need to be overcome in practical applications. First, vibration characteristics are functions of the structural stiffness, mass and damping. Although structural damage can cause an increase or a decrease in modal damping and the removal or loosening of structural components can change mass distribution [5], most of the current modal-based DD algorithms need to ignore the variations of mass and damping for simplicity. Another difficulty is that many mode shape-based DD methods need accurate mode shape estimation, which can be very challenging in real structures. In addition, a number of vibration-based DD methods require high-order modal data and this is another common practical difficulty.

The static responses, on the other hand, are solely related to the structural stiffness as evidenced from the static equilibrium equations. The use of static parameters in damage detection context is therefore straightforward considering stiffness reduction is the main source of structural damage in civil structures. In fact, static deflection has been a fundamental parameter in the SHM of many important structures including bridges. Although measuring vertical deflection in bridges using traditional contacting sensors has long been considered as a challenging task, various alternative non-contact techniques including the emerging vision-based optical techniques have been developed and applied to bridge deflection measurement with promising outcomes for periodic, continuous or even real-time measurement [6-8]. Another advantage of using static deflections is that the sparsity of displacement sensor can be overcome by applying Maxwell's reciprocity theorem [9]. In addition, the static deflections can be measured directly through applying loads on the structures, or estimated indirectly from modal flexibility matrices constructed from dynamic tests [10, 11]. Owing these advantages, the static DD methods have attracted more attention in the SHM field in recent years. Sanayei and Onipede [12] proposed an iterative optimization-based algorithm to identify the structural element stiffness by evaluating the difference between the analytical and the measured static displacements under known static loads. Banan *et al.* [13], Banan *et al.* [14] estimated the member constitutive properties by using constrained least-square minimization method in an iterative manner to minimize the discrepancy between the measured displacement and that from finite element model (FEM). Based on this research, Hjelmstad and Shin [15] proposed an adaptive parameter grouping scheme to locate damage from sparse and noise measurements. Sanayei *et al.* [16] presented an adaptive algorithm of the parameter grouping to detect and assess the damage from experimental static displacement and static strain responses. Wang *et al.* [17] utilized both static testing data and natural frequencies to identify the damage. The damage severity was then estimated using an iterative quadratic programming technique. Bakhtiari-Nejad *et al.* [18] applied an optimization criterion to detect damage in linear elastic structures from static noisy measurement by minimizing the difference between the load vectors before and after the damage. Chen *et al.* [19] used the grey relation coefficient of displacement curvature to locate the damage before using an iterative estimation scheme to estimate the damage extend on cantilever beams. Yang and Sun [20] proposed a static-based damage locating and quantification method using the flexibility disassembly technique and the concept of damage localization vector derived from the static response equation. However, the method requires a refined FEM representing for the undamaged state. Kourehli *et al.* [21] applied the simulated annealing algorithms to solve the objective functions formulated from modal data and static displacement. They were able to locate and quantify damage in beam and frame structures.

All of the above methods used the iterative optimization-based technique and/or require a refined FEM to compute the damage parameters. It is apparent that for high noisy data and/or for multiple damage cases, the iterative algorithms involve multiple iterations in order to provide a precise damage detection results, and this could lead to very high computational cost. In addition, the discrepancy between real structures and the FEM can cause significant errors on the damage detection results. Without the aid of these techniques, some methods can only succeed in locating the damage. Choi *et al.* [9] developed an elastic damage load theorem which is the ratio of bending moment to the flexural rigidity to locate the damage in simply supported beams. However, the method was limited to statically determinate beams, and only single damage cases were discussed. Abdo [22] used the changes in the displacement curvature derived from measured static response and the grey relation coefficient concept to locate damage in beams. As this coefficient does not contain a physical relation to the damage severity, the method cannot directly quantify the damage. Seyedpoor and Yazdanpanah [23] proposed a damage locating concept based on changes in static strain energy of a structure subjected to static load cases. The efforts to locate and quantify damage without relying on the optimization algorithms and a FEM have gained some successes. Grandić and Grandić [24] utilised the grey relation coefficient to identify the damage location, then proposed a damage quantification method from curvature of displacement influence line in simply supported beams. In the field of static-dynamic combination approach, Koo *et al.* [25] and Sung *et al.* [11] successfully located and quantified damage in shear buildings from damage-induced deflection obtained from modal flexibility. However, the techniques are limited to shear buildings and they can be erroneous when applied to bending dominant structures.

Motivated from recent advances in deflection measurement technology, a new static DD method that does not rely on an optimization algorithm or a FEM is proposed in this study for locating and quantifying damage in Euler-Bernoulli beams from static deflection changes. This method aims to address damage in its early sates and therefore falls into the linear damage category in which the structure is assumed linear in the pre- and post-damaged states. For the damage locating concept, the deflection change (*DC*) parameter is formulated as a function of damage characteristics using the principle of Virtual Work. From this, a plot of the measured *DC*

can be observed to identify the damage locations. For the first time, the ability of the *DC* parameter in locating damage is supported by closed-form mathematical functions, which contain both damage location and damage severity information. From these formulas, the damage severity is estimated conveniently without the aids of a FEM or optimization algorithms. The rest of this article is organised as follows. First, the construction of the *DC* functions with respect to the damage characteristics are established, from which the damage locating concept is presented. Next, the relative deflection change as a function of damage severity is derived, from where the damage quantification concept is introduced. Numerical and laboratory investigations are then presented to demonstrate the effectiveness of the proposed method. Finally, the paper discusses practical application aspects, before concluding with some final remarks.

2. Theory

This paper focuses on simply supported (SS) and cantilever Euler-Bernoulli beams. However, the concept can be extended to other beam-type structures including statically determinate and indeterminate beams. As the formulas developed for cantilever beams differ slightly from the SS beams, they are presented separately in the Appendix for brevity. Throughout this paper, damage is assessed in beam segmental level due to the fact that damage occurring at one position will definitely cause stiffness reduction in the surrounding area [26]. The static DD concepts presented herein is not limited to one particular static load case. However, the unit point loads acting at the mid-span of SS beams, or at the free end of cantilever beams are selected for simplicity, and for the fact that they cause maximum deflections compared to other positions, which in turn can minimize the effects of measurement noise.

2.1. Damage detection in simply supported beams with single damage

2.1.1. Damage locating concept for SS beam from static deflection change

Consider a SS beam with constant bending stiffness $(EI)_x = EI$ (Fig. 1a). Under the mid-span unit point load, the undamaged deflection of the beam (u^h) at the beam location x can be formulated from the principle of Virtual Work method [27] by:

$$u^h(x) = \int_0^L \frac{M(x_1).m(x_1)}{(EI)_x} dx_1 = \int_0^L \frac{M(x_1).m(x_1)}{EI} dx_1 \tag{1}$$

where, $M(x_1)$ is the bending moment of the beam due to the real unit point load (Fig. 1b), $m(x_1)$ is the bending moment due to a virtual unit point load acting at x (Fig. 1c). After substituting the moment functions and expanding the integration, the undamaged deformation of the beam is given by Eq. (2).

$$u^h(x) = \frac{1}{12EI} u_0(x) \tag{2}$$

$$u_0(x) = 2\langle x - \frac{L}{2}\rangle^3 + x\left(\frac{3}{4}L^2 - x^2\right) \tag{3}$$

where, $u_0(x)$ is a geometric function containing the inspection coordinate (x) and the beam length (L); the Macaulay bracket $\langle\ \rangle$ should be replaced by ordinary parentheses ( ) when $x \geq L/2$, and by zero when $x < L/2$.

In the damaged state, assuming the beam gets damaged in a single segment $a \leq x \leq a + b$ (Fig. 1d), with the corresponding bending stiffness of $(1 - \alpha)EI$, where $0 \leq \alpha < 1$ is the damage severity coefficient. As the moments in statically determinate beams are independent from member stiffness changes, the deflection of the beam (u^d) under the same unit point load can be formulated from the Virtual Work method by:

$$\begin{aligned} u^d(x) &= \\ &= \int_0^a \frac{M(x_1).m(x_1)}{EI} dx_1 + \int_a^{a+b} \frac{M(x_1).m(x_1)}{(1-\alpha)EI} dx_1 + \int_{a+b}^L \frac{M(x_1).m(x_1)}{EI} dx_1 \\ &= u^h(x) + \int_a^{a+b} \left(\frac{1}{1-\alpha} - 1\right) \frac{M(x_1).m(x_1)}{EI} dx_1 = u^h(x) + \beta \int_a^{a+b} \frac{M(x_1).m(x_1)}{EI} dx_1 \end{aligned} \tag{4}$$

where, β is a damage severity derivative defined by Eq. (5).

$$\beta = \frac{\alpha}{1-\alpha} \tag{5}$$

After expanding the last integration in Eq. (4), the deflection change (*DC*) of the beam is given by:

$$DC(x) = u^d(x) - u^h(x) = \begin{cases} \beta \frac{1}{12EI} B_1 x & , \quad x \le a \quad (6a) \\ \beta \frac{1}{12EI} B_2 (L - x) & , a + b \le x \le L \quad (6b) \end{cases}$$

where, the scalar functions B_1, B_2 are defined as follows depending on the relative position of the damage compared to the load point:

$$a + b \le \frac{L}{2}: \; B_1 = \frac{b}{L}[(2a + b)(3L - 2a - 2b) - 2a^2]; \; B_2 = \frac{2}{L}[(a + b)^3 - a^3] \quad (7a)$$

$$a \le \frac{L}{2} < a + b: \; B_1 = \frac{1}{L}\left[\frac{3}{4}L^3 - 3La^2 + 2a^3 - 2(L - a - b)^3\right]; \; B_2 = \frac{1}{L}\left[(a + b)^2(3L - 2a - 2b) - \frac{L^3}{4} - 2a^3\right] \quad (7b)$$

$$a > \frac{L}{2}: \; B_1 = -\frac{2}{L}[(L - a - b)^3 - (L - a)^3]; B_2 = \frac{b}{L}[(2a + b)(3L - 2a - 2b) - 2a^2] \quad (7c)$$

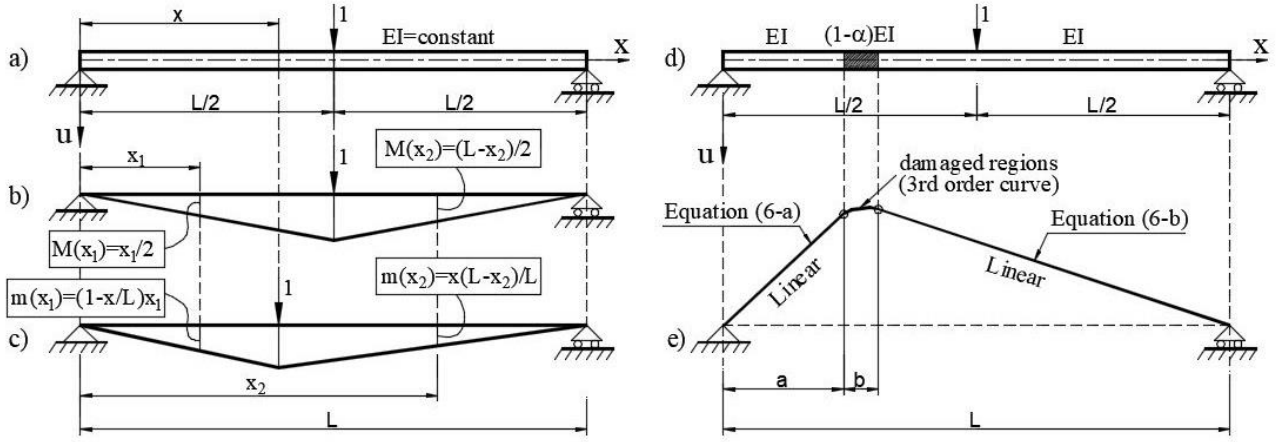

Fig. 1. Damage locating concept of SS beam under single damage: a) Undamaged SS beam configuration; b) and c) Bending moments under real and virtual unit loads; d) Damaged beam configuration; e) Deflection change plot

It should be noted that a third order function of *DC* in the damaged region ($a \le x \le a + b$) is omitted in Eq. (6) for simplicity. By plotting Eq. (6) to Fig. 1e, it is evident that the *DC* encompasses two linear portions starting from the supports towards the damaged element, and hence reaches its maximum values within the damaged region. Therefore, the damaged element can be located based on two indicators, viz. (i) at the "peak" region of the *DC* plot, and (ii) between the two linear portions. As will be illustrated in the numerical and experimental validations, both the indicators can be satisfied in most of the cases, while in some situations the linearity can be less obvious due to measurement noise. In the latter situations, a clear peak region on the *DC* plot can be sufficient to locate the damage.

It should be emphasized that the ability of the static *DC* in locating damage in SS beams has been reported in the literature, such as in Choi *et al.* [9]. However, they used an elastic damage load theorem to explain the *DC* pattern and the method was not able to quantify the damage. In fact, for the first time in this paper, the *DC* is formulated in a mathematical form, which contains both the information of damage location and damage severity, and hence provides a clear theoretical base for the *DC* damage locating concept. More importantly, the formulated *DC* will lead to a new damage quantification method presented in the next section.

2.1.2. Damage quantification for SS beams from relative static deflection change

After the damage is located at segment (a, $a + b$) in previous step, its severity information is essential to enable higher levels of a damage identification process. Eq. (6) characterizes the *DC* of SS beams with respect to a damage severity derivative (β). However, it also contains the stiffness quantity *EI*, which is unknown or not always accurately obtained in practice. In this paper, the stiffness quantity is eliminated by relating the *DC*

function from Eq. (6) to the undamaged deflection function from Eq. (2), yielding the relative deflection change (*RDC*) as follows:

$$RDC(x) = \frac{DC(x)}{u^h(x)} = \beta\ RDC^{50\%}(x) \tag{8}$$

where,

$$RDC^{50\%}(x) = \begin{cases} B_1 x/u_0(x) & , \quad x \le a \\ B_2(L-x)/u_0(x) & , a+b \le x \le L \end{cases} \tag{9}$$

From Eq. (8), it is evident that the scalar function $RDC^{50\%}$ is physically the measured *RDC* of the beam in a special damaged state that causes $\beta = 1$ (or $\alpha = 50\%$) at the same damaged element. This explains the notation $RDC^{50\%}$ and its superscription 50%. The $RDC^{50\%}$ function contains only the geometrical entries and is independent from the damage severity. It is calculated exclusively from the knowledge of the previously identified damage location (*a, b*), in addition to the beam length (*L*) and the coordinate of the inspection points (*x*). This implies that each beam element provides a unique $RDC^{50\%}$ function, which can be calculated after the damaged element is identified. It is also evident from Eq. (8) that the measured *RDC* differs from the calculated $RDC^{50\%}$ by the scalar β at every inspection points. Therefore, the $RDC^{50\%}$ can be considered as a baseline for the measured *RDC* in quantifying the damage.

If the deflections are measured with negligible noise and the damaged element is correctly located, the ratio between *RDC* and $RDC^{50\%}$ at different measurement points should derive the same value, viz. β. In practice, however, as a certain amount of measurement noise is unavoidable, a variation of the $RDC/RDC^{50\%}$ ratio among the inspection locations can be expected. This leads to a new damage quantification concept designated in this paper as the damage severity consistency function, denoted as *DSC(x)*, and defined by:

$$DSC(x) = \frac{RDC(x)}{RDC^{50\%}(x)}\ , \qquad x \notin (a, a+b) \tag{10}$$

A good consistency, i.e. a constant or nearly constant *DSC(x)* function, implies that the damage is correctly detected from less noisy measured deflections (e.g. Fig. 5c). By contrast, a significant variation of the *DSC(x)* function (e.g. Fig. 14a) suggests that the deflections were subjected to high measurement noise. From (8) and (10), the damage severity derivative β can be obtained by averaging the *DSC(x)* as follows:

$$\beta = \overline{DSC(x)}, \qquad x \notin (a, a+b) \tag{11}$$

Finally, from (5) the damage severity at the located damaged element is calculated by:

$$\alpha = \frac{\beta}{1+\beta} \tag{12}$$

From Eqs. (10) to (12), it is evidenced that the damage severity can be calculated directly from the measured *RDC* parameter without the need of an optimization algorithm.

2.2. Simply supported beams with double damage locations

Fig. 2a depicts the beam configuration with two damaged elements and the corresponding stiffness reduction coefficients α_i (i = 1, 2). The *DC* function under the mid-span unit point load can be constructed from the principle of Virtual Work method following an analogous procedure, or by superposition method based on the two separated single damage cases, as follows:

$$DC(x) = \begin{cases} (1/12EI)\left(B_{11}\beta_1 + B_{12}\beta_2\right)x & , \quad x \le a_1 & \text{(13a)} \\ (1/12EI)\left(B_{21}\beta_1 + B_{22}\beta_2\right)(L-x)\ , & x \ge a_2 + b_2 & \text{(13b)} \end{cases}$$

where, the scalars B_{1i}, B_{2i} are defined from (7) for the i^{th} damage location. It should be noted that another linear function of *DC* in the region $a_1 + b_1 < x < a_2$, and two third-order functions in the damaged regions are omitted from (13) for simplicity. Fig. 2b depicts the damage locating concept for the double damage case based on a measured *DC* plot, in which the left and the right portions correspond to Eq. (13a) and (13b), respectively. It is evident that the damage locations can be detected at the two abrupt changes between the three linear portions.

From (13) and (2), the *RDC* function is derived as:

$$RDC(x) = \begin{cases} \beta_1 RDC_1^{50\%}(x) + \beta_2 RDC_2^{50\%}(x), & x \le a_1 \\ \beta_1 RDC_1^{50\%}(x) + \beta_2 RDC_2^{50\%}(x), & x \ge a_2 + b_2 \end{cases} \quad (14)$$

where, the $RDC_i^{50\%}$ is the baseline *RDC* function calculated for the i^{th} damaged element by (i= 1, 2):

$$RDC_i^{50\%}(x) = \begin{cases} B_{1i}x/u_0(x) & , \quad x \le a_i \\ B_{2i}(L-x)/u_0(x) & , a_i + b_i \le x \le L \end{cases} \quad (15)$$

Similar to the single damage case, the damage severity consistency functions for the two damaged elements can be given by:

$$DSC_i(x) = \frac{RDC(x)}{RDC_i^{50\%}(x)}, \quad x \notin (a_i, a_i + b_i), \quad i = 1,2 \quad (16)$$

Eq. (14) is therefore can be rewritten as:

$$\begin{cases} (1/DSC_{11})\beta_1 + (1/DSC_{12})\beta_2 = 1, & x \le a_1 \\ (1/DSC_{21})\beta_1 + (1/DSC_{22})\beta_2 = 1, & x \ge a_2 + b_2 \end{cases} \quad (17)$$

where,

$$\begin{cases} DSC_{1i} = \overline{DSC}_{1i}(x) = \overline{RDC(x)/RDC_i^{50\%}(x)}, & 0 < x \le a_1, i = 1,2 \\ DSC_{2i} = \overline{DSC}_{2i}(x) = \overline{RDC(x)/RDC_i^{50\%}(x)}, & a_2 + b_2 \le x < L, i = 1,2 \end{cases} \quad (18)$$

The damage severity derivative β_i can be obtained easily by solving (17). Finally, the damage severity coefficients α_i are calculated from Eq. (12) for each of the two damage locations.

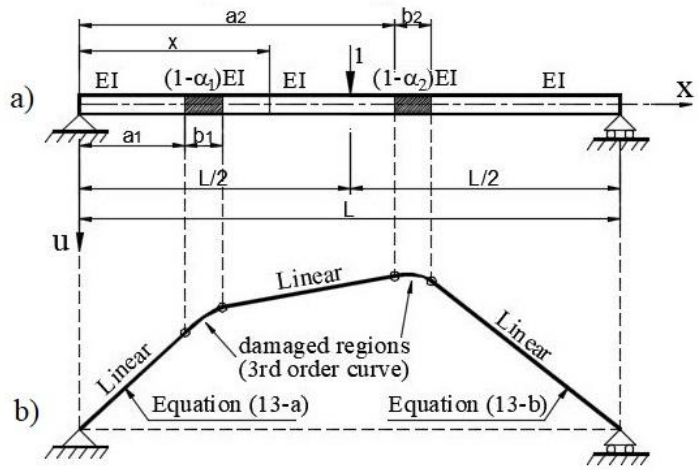

Fig. 2. Damage locating concept of SS beam under double damages:
a) Undeformed SS beam, b) Deflection change plot

2.3. Procedure for locating and quantifying damage in SS beams using *DC* and *RDC*

The procedure for locating and quantifying elemental damage in SS beams using *DC* and *RDC* obtained from static tests can be summarised as follows:

1. Scale the measured deflections in the undamaged and suspected states to be under the unit point load
2. Calculate the *DC* and *RDC* vectors
3. Plot the *DC* curve and locate the damage following the proposed damage locating concept
4. Based on the obtained damage location identifiers *(a, b)* in previous step, calculate the $RDC^{50\%}$ function from (9) for single damage, or from (15) if two damages are identified
5. Calculate the *DSC(x)* function from (10) for single damage, or (16) for double damage case
6. Calculate β from (11) or (17) depending on the number of damage location
7. Obtain the damage severity coefficient α from (12).

3. Case study 1 - Numerical investigation for SS beam

3.1. Numerical model

A 24 m simply supported reinforced concrete beam is modelled using the finite element (FE) software package SAP2000 (Fig. 3). The Young's modulus, Poisson's ratio and mass density for the material are 35 GPa, 0.2 and 2500 kg/m^3, respectively. The second moment of area of the cross-section is 0.5 m^4. Four damage scenarios are simulated by reducing the material Young's modulus, in which the first three scenarios are single damage cases at the same element but with increasing damage severities, and the last is a double damage case (Table 1). This modelling technique can represent for general damage related to flexural stiffness reductions.

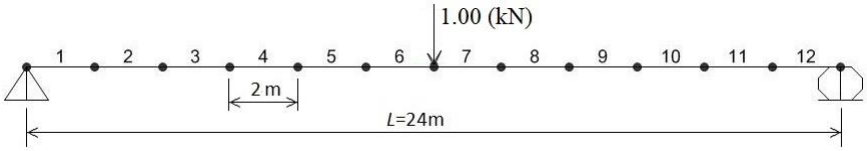

Fig. 3. FE model of the beam

The deflections of the beam in the healthy and damaged states under the same unit point load (1 kN) acting at the mid-span are plotted in Fig. 4. The increasing trend in the deflections suggests the presence of cumulative damage. However, this does not provide enough information to locate and quantify the damage. Further investigation is therefore needed.

Table 1. Damage scenario definition for Case study 1

Damage case	D1.1	D1.2	D1.3	D1.4	
Damaged element(s)	6	6	6	6	9
Simulated damage severity (flexural stiffness reduction)	10%	20%	30%	30%	30%

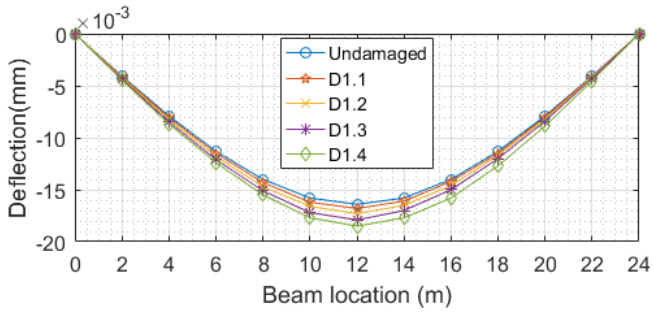

Fig. 4. Deflections of the beam under the mid-span unit point load

3.2. Damage detection result for single damage cases

Fig. 5 illustrates the damage detection results for the three single damage cases. Fig. 5a plots the *DC* vectors obtained from the measured deflections before and after damage. As expected, the *DC* plots encompass two linear portions and a "peak" region at element No.6 in all three damage scenarios. This element is therefore identified as the damaged element according to the theory section. It is evident from Fig. 5a that the intensity of the *DC* plots are proportional to the damage severities, i.e., highest for D1.3, and lowest for D1.1. This accurately reflects the theoretical relationship between *DC* and the damage severity coefficient developed in Eq. (6). The damage location identifiers are then determined as a = 10 m and b = 2 m, and the corresponding scalars B_i are calculated from (7a) as B_1 = 71.33 and B_2 = 60.67, which are independent from the damage severity.

To estimate the damage severity, the baseline $RDC^{50\%}$ vector is calculated from (9) and plotted as in Fig. 5b, together with the measured *RDCs*. It is evident that the measured *RDC*s are proportional to the baseline $RDC^{50\%}$, and that the intensity of the *RDC* plots is proportional to the damage severity, i.e., highest at $RDC^{50\%}$ (severity = 50%), then D1.3 (30%), D1.2 (20%), and lowest at D1.1 (10%). The corresponding damage severity consistency functions *DSC(x)* are calculated as the ratio of the measured *RDC*s to the baseline $RDC^{50\%}$ following (10). Fig. 5c indicates that *DSC(x)* is a constant for each of the damage scenarios, viz. 0.1108, 0.2496 and 0.4268 for D1.1, D1.2 and D1.3, respectively. This is expected because the measured deflections are noise-free and the damage was correctly located. Finally, from (11) and (12), the damage severity coefficients are

accurately calculated as 9.97% for D1.1, 19.9% for D1.2 and 29.91% for D1.3 (Fig. 5d), with minor errors compared to the simulated severities (Table 1).

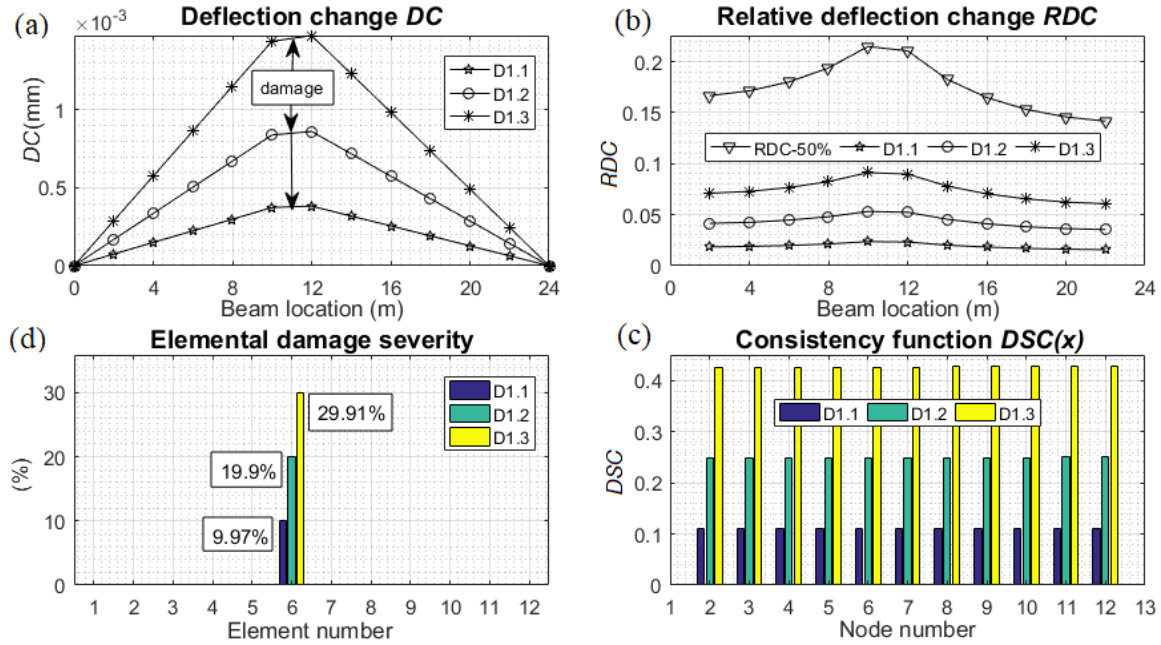

Fig. 5. Damage detection results - Case D1.1-D1.3: (a) Locating damage from the *DC* plots, (b) Relative deflection change, (c) Damage severity consistency functions, (d) Estimated damage severities

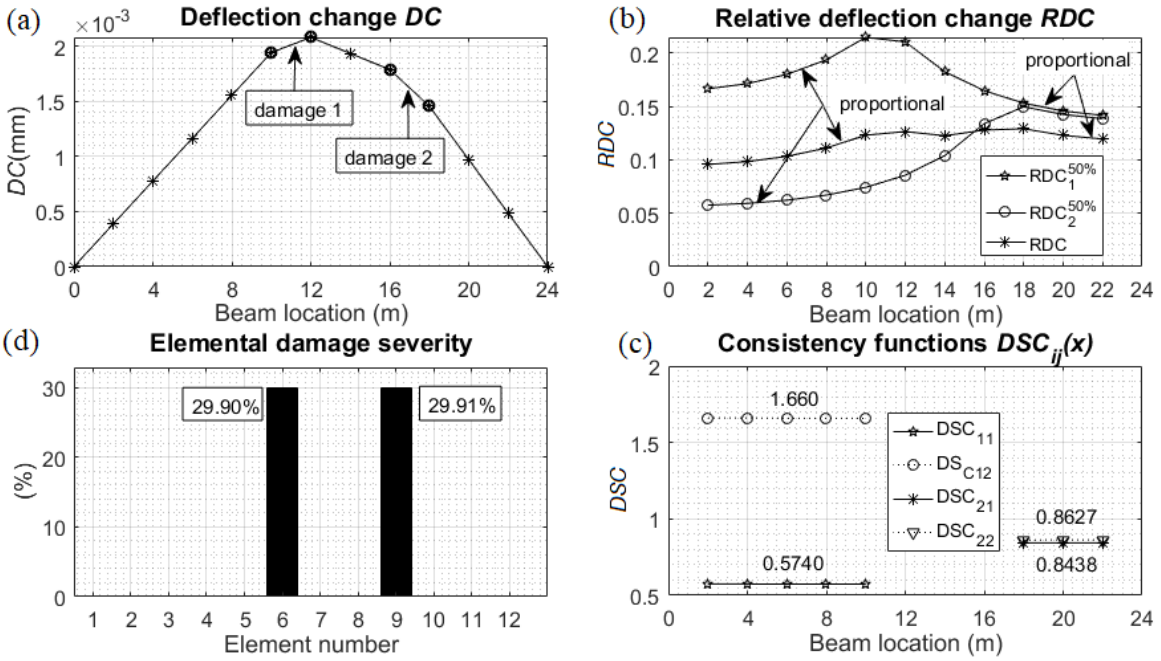

Fig. 6. Damage detection result – Case D1.4: (a) Locating damage from the *DC* plot, (b) Relative deflection change, (c) Consistency functions, (d) Estimated damage severities

3.3. Damage detection results for the double damage case

Compared to the preceded single damage cases, the damage quantification process in this double case requires some differences in the last steps. After the damaged elements are identified at the abrupt changes of the *DC* plot (Fig. 6a), the scalars B_{1i} and B_{2i}, and the two scalar functions $RDC_i^{50\%}$ (i = 1, 2) are calculated following Eqs. (7) and (15). Fig. 6b illustrates the baseline $RDC_i^{50\%}$ and the measured *RDC* plots for D1.4. It is apparent that the measured *RDC* is proportional to the baseline $RDC_i^{50\%}$ in the regions x ≤ 10 m and x ≥ 18 m. This resulted in the corresponding consistency functions $DSC_{ij}(x)$ calculated from (16) and plotted in Fig. 6c. On

the substitution of the average *DSC* values (DSC_{11} = 0.5740, DSC_{12} = 1.660, DSC_{21} = 0.8438, DSC_{22} = 0.8627), Eqs. (17) turn to:

$$\begin{cases} (1/0.5740)\beta_1 + (1/1.660)\beta_2 = 1\ , & x \le 10 \\ (1/0.8438)\beta_1 + (1/0.8627)\beta_2 = 1\ , & x \ge 18 \end{cases}$$

The solution of the equations yields β_1 = 0.4265, β_2 = 0.4267. Finally, the damage severities are calculated as α_1 = 29.90% and α_2 = 29.91%, with minimal errors compared to the simulated severities (Fig. 6d).

4. Case study 2 - Experimental verification for SS beam

4.1. Test descriptions and damage scenarios

The laboratory test used in this study was conducted in the Structural Laboratory at Queensland University of Technology with support from the university Design and Manufacturing Centre. The testing model consists of an AS/NZS grade C450 cold formed Duragal 75×40×4 CC beam channel section, which was supported by a pinned and a roller supports to simulate the structural behaviours of simply supported beams (Fig. 7). For experimental verification, the beam was tested under static point loads acting at the mid-span in order to capture its deflections in the healthy and various damaged states (Fig. 8). The supports were designed so that they carry the beam at the neutral axes of the cross-section. Damage was simulated by cutting the two flanges by 1.5 mm width cuts, with varying depths in an incremental manner (Fig. 9). The actual dimensions of the beam's cross-section are illustrated in Fig. 9.

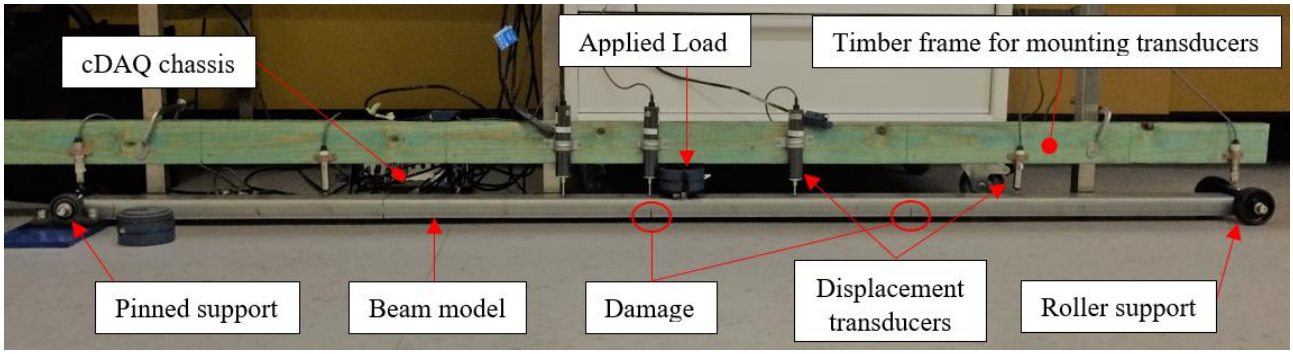

Fig. 7. The laboratory simply supported beam model

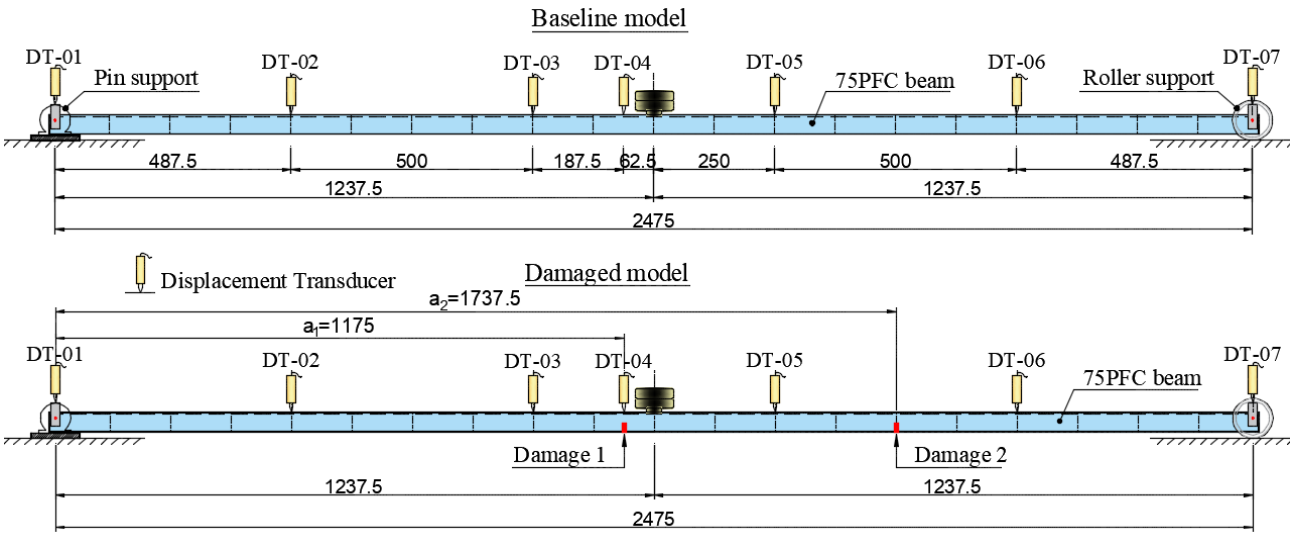

Fig. 8. Schematic diagram of the test model in baseline and damaged states (length in mm)

Prior to the static testing, the data acquisition system was established, which included seven strain gauge-type displacement transducers (DTs) positioned to measure the beam vertical displacements. The data acquisition system including a NI cDAQ 9172 chassis, two NI 9237 bridge input modules, and eight NI 9949 terminal blocks to form eight measurement channels. In addition, an in-house LabVIEW professional app was used to read and log the data in a fully synchronized and automated acquisition manner. The transducers were sampled

under the rate of 2000 Hz as the minimum allowable sampling rate of the NI 9237 modules is 1613 Hz [28].

The static test was conducted in the undamaged state of the beam (D2.0), which is considered as baseline structure. Then five static tests numbered from D2.1 to D2.5 were carried out in the damaged states. Each of the tests was conducted repeatedly for 25 measurements under the same 2.1 kgf point load at the mid-span, and then the average results were used. Each measurement lasted for 60 seconds, of which the first 20 seconds were without loads, the next 20 second were for loading time, and the last 20 seconds were in the loaded condition. The difference between the averaged displacement of the last 20 seconds and that of the first 20 seconds provides the beam deflection.

Free vibration test was also conducted during the static test without added mass in order to capture free vibration characteristics of the beam. These parameters were used to verify the beam properties. Only frequency results from the vibration test in the undamaged state are presented herein (Table 6) as the focus of this paper pertains to damage detection using static deflection changes.

Damage case	Damage 1		Damage 2	
	x_1 (mm)	hc (mm)	x_2 (mm)	hc (mm)
D2.1	1175	8.5		
D2.2	1175	12.5		
D2.3	1175	18		
D2.4	Same as D2.3		1737.5	12
D2.5	Same as D2.3		1737.5	18

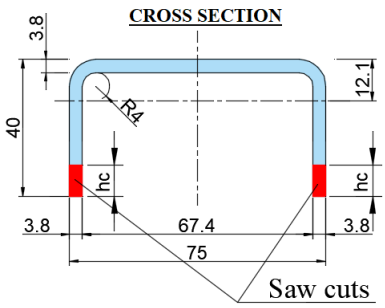

Fig. 9. Damage scenario definition (length in mm; to be seen with Fig. 8)

4.2. Test results

The beam was also tested under different loading magnitudes and the deflections were correlated with very good linearity. This allows one to scale the measured deflections under the tested load (2.1 kgf) to an equivalent unit point load of 1 N (step 1 of the proposed DD procedure, section 2.3). The scaled deflections are listed in Table 2. Again, these deflections are the average values from 25 measurements conducted in each state. The corresponding deflection curves are plotted in Fig. 10, which show a clearly accumulated trend. The state of damage is therefore discernible. However, this does not yet provide any indication of the damage location and the damage severity. Therefore, more advanced damage assessment is required.

Table 2. Deflection of the beam under an equivalent 1 N mid-span load ($\times 10^{-3}$ mm)

Sensor No.	X (mm)	D2.0	D2.1	D2.2	D2.3	D2.4	D2.5
DT-01	0	0.166	0.179	0.181	0.167	0.215	0.189
DT-02	487.5	9.850	9.924	10.129	10.603	10.609	10.828
DT-03	987.5	16.117	16.422	16.787	17.568	17.739	17.982
DT-04	1175	16.897	17.260	17.758	18.593	18.792	19.111
DT-05	1487.5	16.090	16.301	16.731	17.459	17.563	18.093
DT-06	1987.5	9.475	9.576	9.717	10.133	10.223	10.647
DT-07	2475	0.014	0.004	0.028	0.026	0.065	0.029

The coefficient of variation (CV) of the 25 measurement are presented in Table 3, which indicates a good level of repeatability (CV<1%). To further aid numerical study, the measurement noise of the test in the undamaged state is calculated for each sensor location as follows:

$$\rho_i = \frac{\max_j \left| X_{ij} - \bar{X}_i \right|}{\bar{X}_i} 100\% \tag{19}$$

where, ρ is the measurement noise level, X_{ij} is the deflection at the i^{th} sensor in the j^{th} measurement (j = 1 to 25), $\bar{X}_i$ is the mean deflections value at the i^{th} sensor. Table 3 summarises the results of measurement noise at each sensor locations, except for the sensors on the supports. Therefore, a 3.5% noise level can be adopted to represent for the measurement noise of the test. This will be used later in Case study 3 to generate laboratory-

like data from numerical deflections.

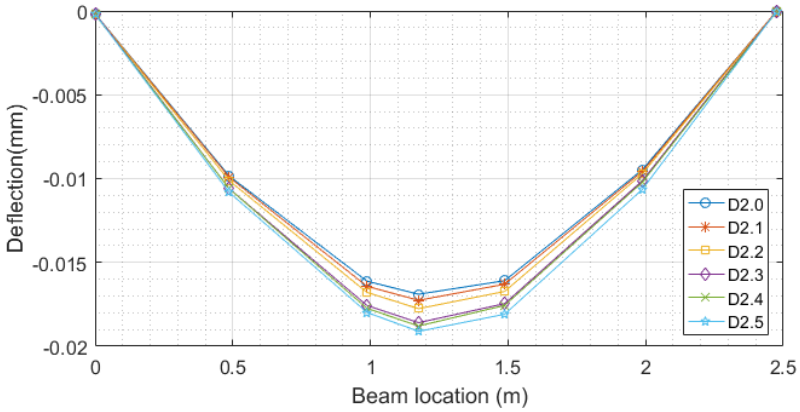

Fig. 10. Deflections of the beam in different damaged states under an equivalent 1 N load

Table 3. Coefficient of variation (CV) and noise level (ρ) of the deflection measurements

Sensor name	DT-02	DT-03	DT-04	DT-05	DT-06
CV (%)	0.69	0.74	0.79	0.76	0.84
ρ (%)	2.83	2.93	2.90	3.06	3.59

4.3. Finite element model validation

In this laboratory test, damage was created by cutting the beam at a sectional manner rather than for a beam element. Hence, the actual elemental damage severity is not known in advance. To verify the accuracy of the experimental results, a finite element model (FEM) of the beam representing for the undamaged state will be validated based on the testing data, then used to simulate the damage in the same way as the test. Damage detection results from the validated FEM (similar to the case study 1) will be used as a reference for those obtained from the laboratory testing. The FEM is developed using the solid elements in the SAP2000 software package (Fig. 11).

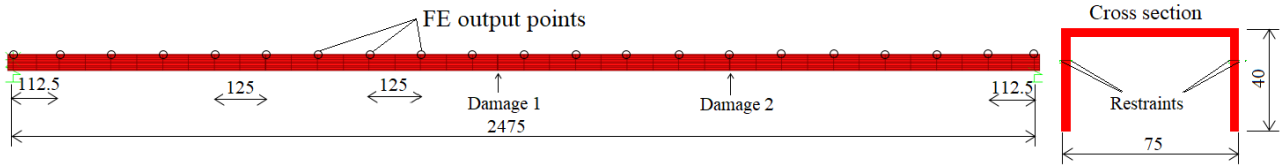

Fig. 11. Finite element model of the experimental beam (dimensions in mm)

As static deflections solely depends on stiffness parameters, the FEM can be simply updated with regard to the beam and the support stiffness. From the basic knowledge of Static Structural Analysis, these stiffness parameters can be conveniently estimated from the measured static deflections as illustrates in Fig. 12. The updating results are shown in Table 4. It is evident that the updated material Young's modulus is in the normal range of cold-formed steel channel sections. In addition, the pin support was more flexible in vertical direction than the roller support.

Table 4. Beam stiffness updating results

Parameter	E (kN/mm^2)	k_1 (N/mm)	k_2 (N/mm)
Updated value	216	3015	35957

Table 5 and Fig. 13 compare the deflection of the beam from the updated FEM and that obtained from the test in the undamaged state. To be comparable, the experimental deflection was interpolated using the shape preserving piecewise cubic interpolation method available in the Matlab software. Table 5 shows that the difference between the experimental and FEM deflections is less than 3.5%, except for x = 237.5 mm where the error is 6.8%, which demonstrates a very good correlation of the results. Vibration characteristics were also compared with good agreement of less than ± 5% difference as shown in Table 6. It is therefore can be concluded that the updated FEM is a good representative for the laboratory model, and the damage detection

conducted in the FEM can be used as a reference for those obtained from the experimental results.

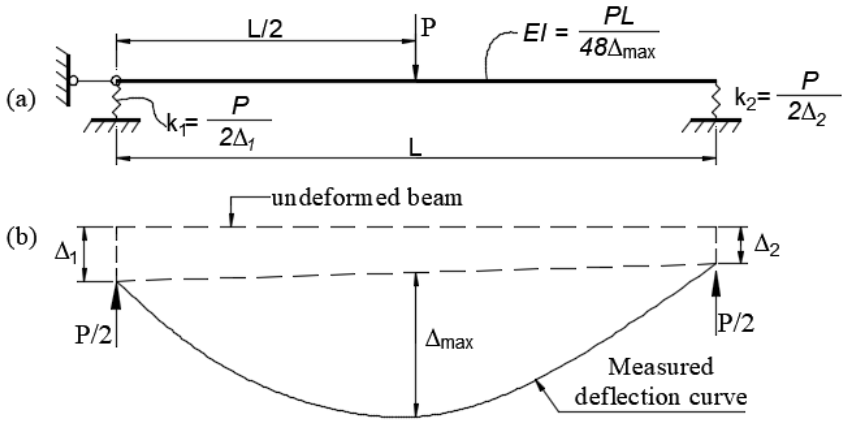

Fig. 12. Schematic of the stiffness updating from measured deflection

Table 5. Deflection of the beam under 1 N mid-span load: FEM verses experiment (deflection in 10^{-3} mm)

X (mm)	0	237.5	487.5	737.5	987.5	1237.5	1487.5	1737.5	1987.5	2237.5	2475
Experiment (*)	0.166	5.376	9.850	13.583	16.117	16.854	16.090	13.510	9.475	5.031	0.014
FEM	0.166	5.010	9.713	13.571	16.165	17.108	16.105	13.452	9.564	4.859	0.014
Error (%)	-0.1	-6.8	-1.4	-0.1	0.3	1.5	0.1	-0.4	0.9	-3.4	1.7

(*) Interpolated from Table 2 *(D2.0)*

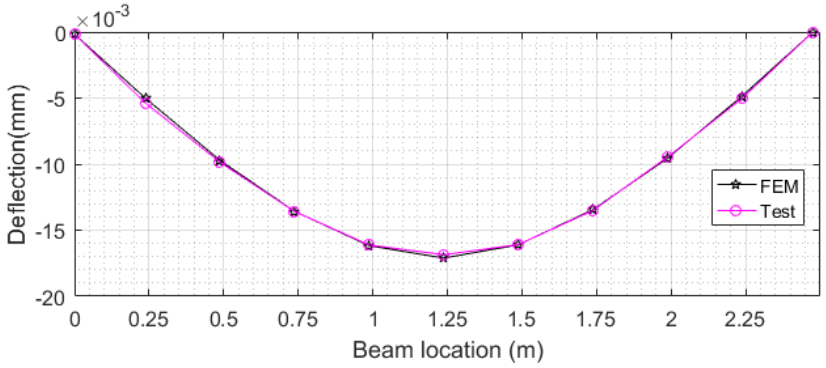

Fig. 13. Deflection of the beam under 1 N mid-span load: FEM verses Test

Table 6. Natural frequencies of the beam: FEM verse experiment

Mode	1	2	3	4
Experiment (Hz)	16.56	62.54	146.31	247.82
FEM (Hz)	16.58	65.13	142.86	241.59
Error (%)	0.12	4.14	-2.36	-2.51

4.4. Damage detection results

Due to the use of small number of displacement transducers, the measured deflections are interpolated into 21 nodes at a spacing of 125 mm, which are the same as those from the FEM.

The damage detection results for the first three single damage cases are shown in Fig. 14. For convenience, results from the validated FEM are plotted together with those from the experiment. The *RDC* and $RDC^{50\%}$ plots are omitted in the subsequent figures for brevity. For the FEM results, in all cases, changes in the deflection (*DC* subplots) clearly indicate a "peak" over the 125 mm long beam element No.10. This element is therefore suspected as the damaged element according to the proposed damage-locating concept. In addition, all the three *DC* plots illustrate linear portions on both sides of the "peak" as expected. This has resulted in the constant values of the *DSC* functions for each of the damage scenarios as shown in the blue bar charts in the second row of the figure. Based on the average values of the *DSC* functions, the damage severities are estimated

at 10.41%, 20.71% and 39.96% for D2.1, D2.2 and D2.3, respectively. These results will be regarded as an approximate reference for the laboratory test.

Regarding the laboratory test, for the two less significant damage cases D2.1 and D2.2 (Fig. 14a, b), unavoidable measurement noise (Table 3) seems to cause noticeable non-linearity of the *DC* plots compared to the FEM results. Nevertheless, the experimental *DC* plots clearly depict a peak region at the beam element No.10. According to the proposed damage locating concept, this element is correctly detected as the damaged element. Although the non-linearity of the *DC* plots resulted in the fluctuation of the subsequent *DSC* plots, using the proposed technique presented in Eqs. (10) to (12), the damage extents were reasonably estimated, with less than ± 2% differences compared to the numerical references.

For the third damage case D2.3 (Fig. 14c), the testing results show satisfactory linearity on the *DC* plots, in addition to a clear peak at the beam element No.10. This can be explained by the fact that the damage-induced *DC* in this case is significant enough that can outweigh the deflection variations due to measurement noise. Consequently, the method accurately locates the damage and quantifies its severity of 41.51%, with minimal difference compared to the FEM result. It also can be observed from Fig. 14 that cumulative *DC* and *DSC* magnitudes from D2.1 to D2.3 clearly indicates the ability of the proposed method in capturing the growth of damage.

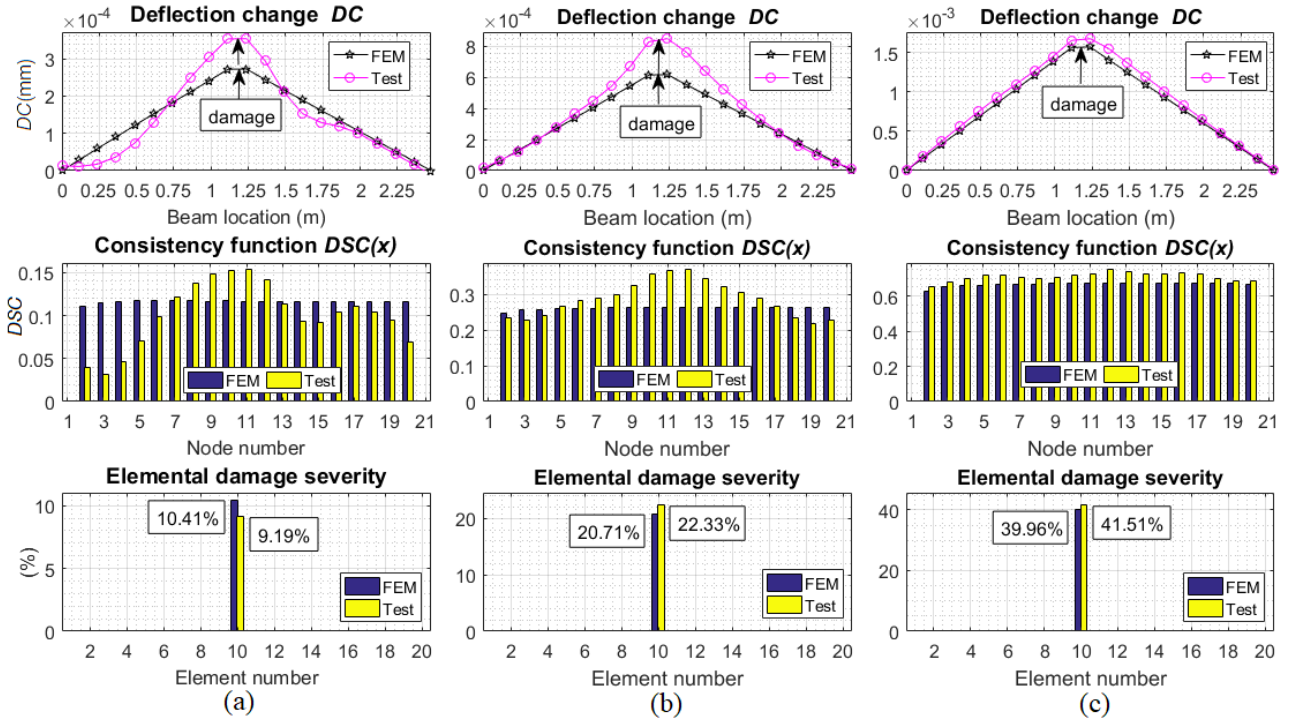

Fig. 14. Damage detection result for: (a) D2.1, (b) D2.2, (c) D2.3

The next damage scenario D2.4 was created from the last single damage case D2.3 by adding another 12 mm cut at 3/4 region of the beam. This new cut is approximately the size of the cut in the second damage case D2.2. Fig. 15a indicates the damage detection results from the noise-free FEM deflection change. The two damaged elements are clearly located based on the proposed damage locating concept. As expected, the estimated damage severity at the first cut almost remains unchanged in comparison with the case D2.3 (39.31% compared to 39.96%), and the result for the second cut approximates that of the case D2.2 (20.56% compared to 20.71%). These results are regarded as the reference for the laboratory test. However, the experimental *DC* plot in Fig. 15b does not provide a clear enough peak at the second damage. Therefore, only the damage in the middle of the beam is detected with confidence. This can be explained by the fact that the sensors are located far away from the actual damage location (Fig. 8), and that it is a common problem in SHM when a small damage is more challenging to detect compared to a larger one. By accepting this damage locating result, the *DSC* function and the damage severity results are shown in the second and third sub-plot of Fig. 15b. It shows that since the second damage is missed, it causes an overestimated result for the first damage when a 43.90% is detected compared to the reference 39.31%.

The damage detection results for the last damage scenario D2.5 are shown in Fig. 16. It is evident that the first

damage is clearly detected at element No.10 for both FE and experimental studies. The second damage is also clearly detected at the beam No.14 in FE study due to the dense grid of output points, while the testing result can only provide a relative damage position between sensors DT-05 and DT-06 because of the coarse sensor arrangement. The beam element No.15 is therefore selected as the second damage in the experimental study. This does not significantly reduce the accuracy of the damage locating result as the actual cut is positioned between beam No.14 and 15. In fact, the resultant *DSC* plot shows a good consistency among the nodes, and the damage severities are estimated with acceptable errors of less than ± 2% difference between FE and the test results (last row of Fig. 16).

To conclude the laboratory case study, the proposed method has shown its robustness in locating and quantifying single damage cases. For the double damage cases, the method can predict the damage locations and estimate the damage extents with satisfactory accuracy when the two damages are equally significant. However, there is some difficulty in using the method when one of the damage is much smaller than the other. In this particular case, only the bigger damage was more clearly detected and its severity was somewhat overestimated.

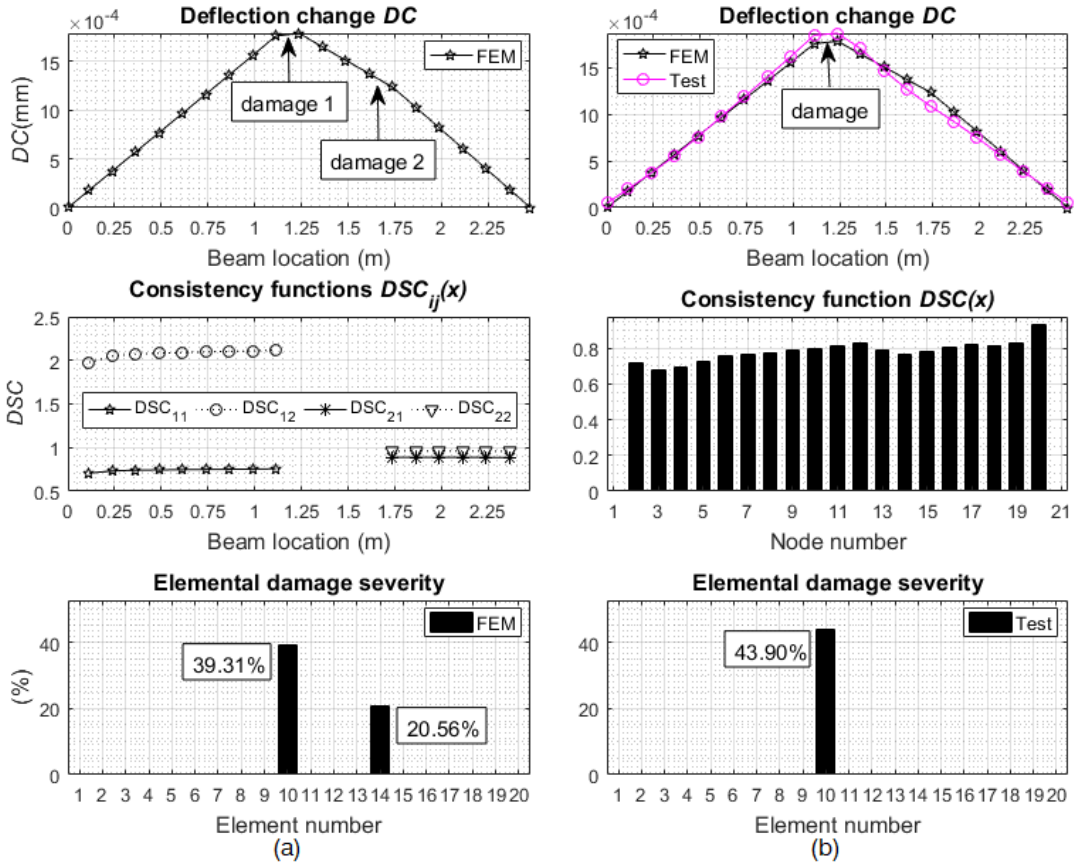

Fig. 15. Damage detection result for D2.4: (a) FEM, (b) Test

5. Case study 3 - Numerical investigation of cantilever beam with noise effect

This case study is conducted in a FE cantilever beam model, with artificial measurement noise added to the deflections. The beam model was developed in the SAP2000 software package using the same cross-section and material properties as those used for the SS beam model in case study 2. The beam cross-section is inverted so that the flanges are in tensile stress area under vertical loads (Fig. 17). The deflection of the beam under a unit point load acting at the tip is used as being representative of the undamaged state. Three damage scenarios are simulated by cutting the vertical flanges in different depths (Table 7), which are the same levels as those conducted for the single damage cases in the SS beam test (refer to Fig. 9). The position of the cuts is at 562.5 mm from the fixed support. Similar to Case study 2, the damage in this section will be quantified for an equivalent stiffness reduction across a length of 125mm (Fig. 17)

As the geometrical and material properties are exactly the same as those from the laboratory SS beam model, the 3.5% noise level calculated from section 4.2 can be used to generate virtual testing data without the need of conducting a similar experiment. The contaminated deflection is calculated in the present work as follow:

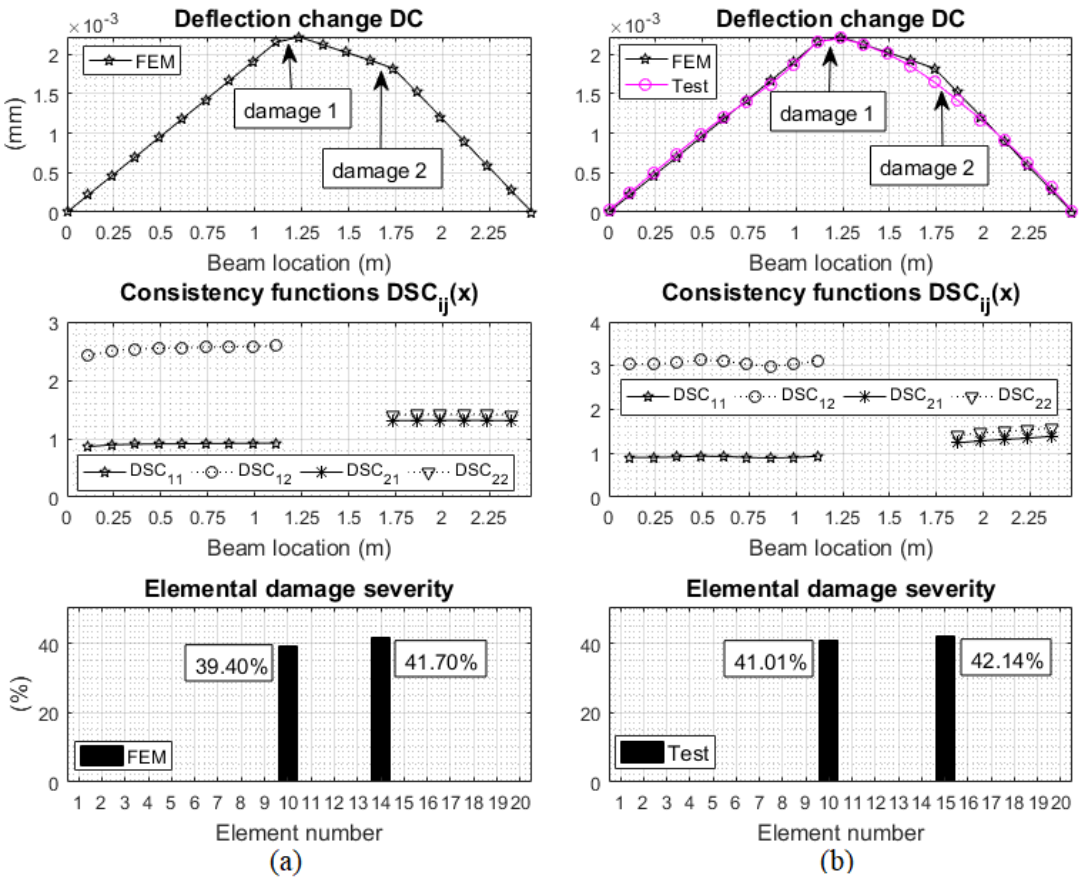

Fig. 16. Damage detection result for D2.5: (a) FEM, (b) Test

$$\tilde{U} = U(1 + \gamma\rho) \tag{20}$$

where, $\tilde{U}$ and U are the deflection at one node with and without noise, respectively; γ is an independent random number in the range of [-1, 1] for that node; ρ is the noise level. In each state, a population of 25 data is generated randomly to simulate the actual test, and the averaged results are used. In order to evaluate the effect of the same noise level to the increasing damage severity, the same set of γ is used for the three damage scenarios. It should be noted that the γ set for the undamaged state is different from that for the damaged states. The deflection changes with and without noise are used to assess the damage using the proposed method for cantilever beams, which is presented in the Appendix.

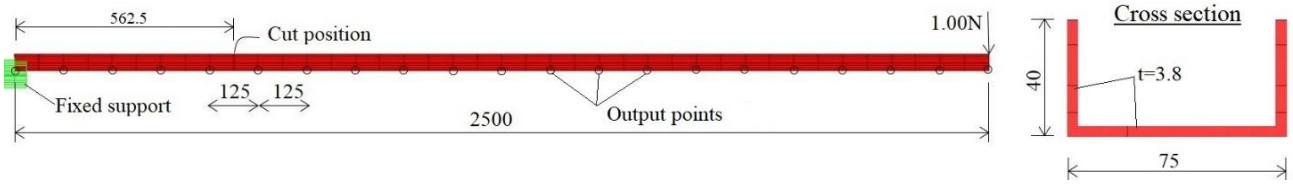

Fig. 17. FE model of the beam (dimensions in mm)

Fig. 18 illustrates the damage detection results, and Table 7 summarises the estimated damage severities. Without noise effects, the *DC* plots increase linearly from the beam location x = 0.625 m towards the free end, which correctly reflects the established theoretical *DC* function. The damaged element is therefore located at the beam element No.5 (x = 0.5 ÷ 0.625 m) according to the proposed damage locating concept. As expected, the resultant DSC(x) functions show constant values among the measurement points, viz, 0.115, 0.268, and 0.681 for D3.1, D3.2 and D3.3, respectively (the blue *DSC* bar charts). This has led to the estimated damage severities of 10.28% (D3.1), 21.14% (D3.2) and 40.52% (D3.3). It is evident that these damage extents are almost the same as those estimated in case study 2 for the same saw cut sizes (refer to Fig. 14). Therefore, the method can accurately quantify the same damages regardless of the beam type.

Table 7. Damage scenarios and damage detection results

Damage case	Depth of the cut (mm)	Estimated damage severity for cantilever beam (%)			
		Noise-free	3.5% noise	7% noise	7% noise using curve fitting technique
D3.1	8.5	10.28	12.36	8.78	9.60
D3.2	12.5	21.14	22.78	18.99	19.08
D3.3	18	40.52	41.49	39.26	39.43

For the results with noise effect, it is apparent that the *DC* plots cannot maintain its linearity. However, the noise only causes considerable fluctuations in the *DC* and *DSC* plots for the smallest damage case, D3.1. For the other more severe cases, D3.2 and D3.3, the noise has negligible effects on the damage locating results. These are similar to the DD results from the laboratory test in the case study 2. The subsequent damage severity estimations show very good results of less than ± 2.5% difference compared to the corresponding noise-free cases.

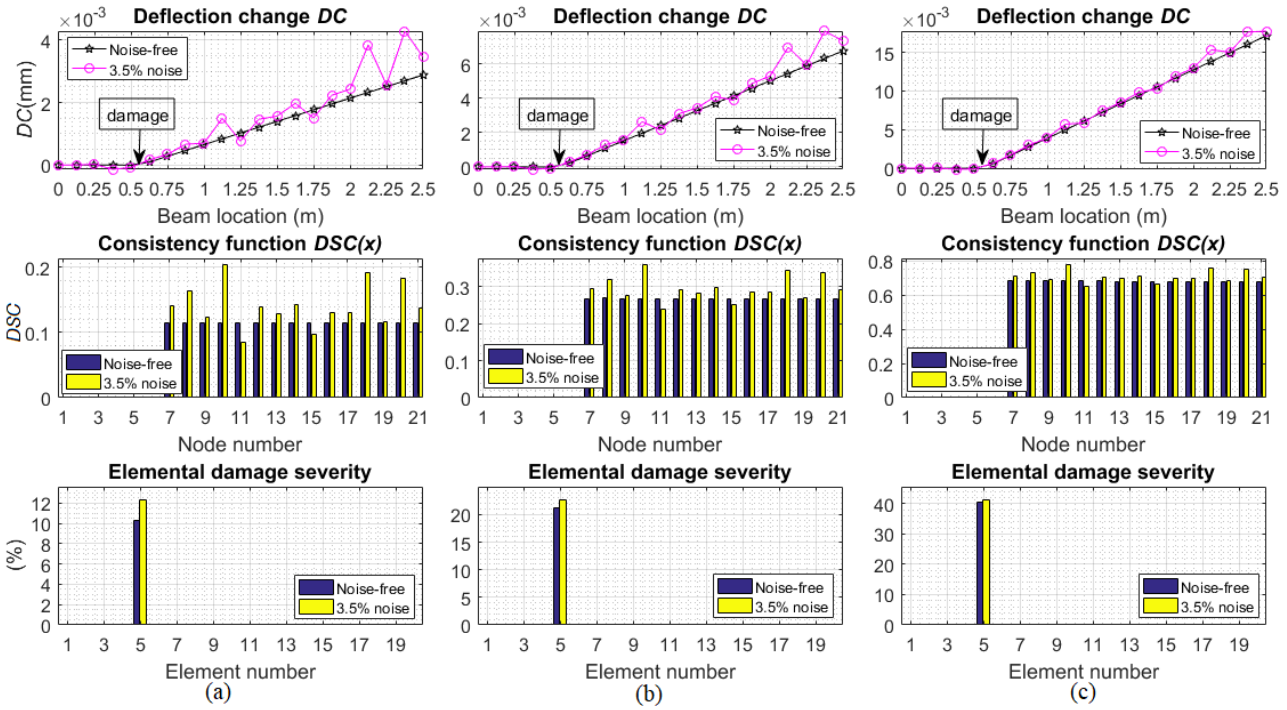

Fig. 18. Damage detection result in noise-free and 3.5% noise level: (a) D3.1, (b) D3.2, (c) D3.3

In an effort to examine the competency of the method under higher noisy condition, a 7% noise level is added to the FEM deflections. For comparison purposes, a simple linear polynomial curve fitting technique is used to fit the distorted *DC* plots in order to reduce the impact of noise before the fitted data is used for damage detection. Fig. 19 compares the DD results of the noise-free and the 7% noise with and without using the fitting technique. The corresponding damage quantification results are summarised in Table 7.

From Fig. 19 and Table 7, it is evidenced that the method retains its robustness in locating and quantifying the damage of larger than 20% severity (D3.2, D3.3), even without using the fitting technique. For the smallest damage case (D3.1), although the distorted *DC* plot cannot provide a clear pattern that matches the proposed damage locating concept, the fitted *DC* plot clearly indicates an increasing trend from x = 0.75 m towards the free end. The damage is therefore detected at the beam element No.6 compared to the simulated No.5, which is acceptable for this early damage state. In all cases, the errors of the estimation results compared to those of the noise-free cases are within ± 3% difference, which demonstrates a satisfactory accuracy.

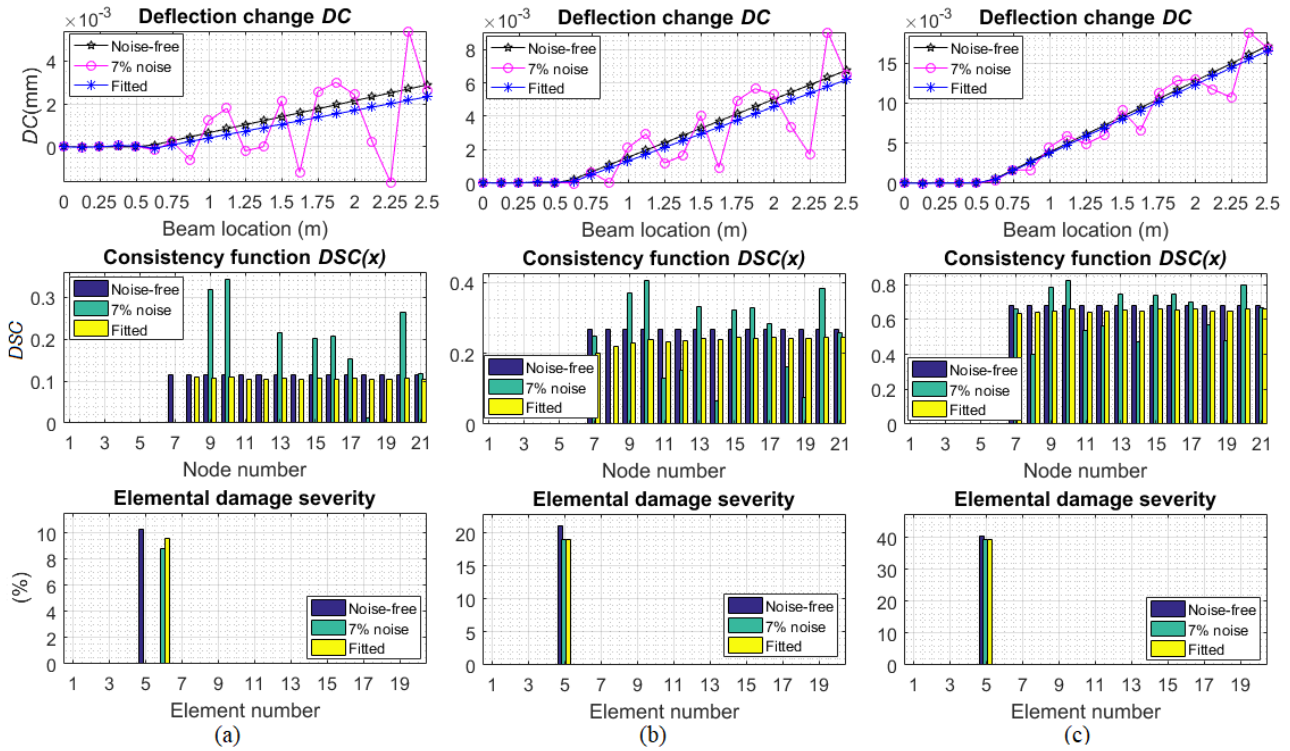

Fig. 19. Damage detection results for 7% noise level: (a) D3.1, (b) D3.2, (c) D3.3

6. Discussions on practical applications

Following the successes of numerical and experimental investigations, future validations on large-scale and full-scale structures would be helpful to gain more understanding on the capabilities of the proposed method under different field conditions. Targeting applications on real bridges, the following practical aspects are worth discussing.

This paper presents damage detection concepts using static deflections under a unit point load applied at a certain location of the beam. However, the method can be generalised to an arbitrary point load or a set of point loads with suitable modifications on the $RDC^{50\%}$ function. In addition, in practice, the deflections can be measured directly or indirectly, with or without the need to apply a specific load on the structures. For example, deflections of a bridge can be measured directly by applying test trucks in non-traffic conditions, such as during the night time [8]. An indirect approach to obtain static deflections without the need of applying a specific load is through modal flexibility matrices constructed from dynamic tests [10, 11]. The former approach can be carried out periodically or after extreme events such as earthquakes and hurricanes when the safety of a bridge is concerned, while the latter approach is applicable for continuous monitoring.

Temperature, as the main environmental factor, can cause difficulties in identifying structural damage, especially in its early states. The need to distinguish between changes resulting from damage and those changes resulting from temperature variations is apparent for any damage detection method [2, 29]. Various techniques have been proposed by researchers to address this problem. The fundamental idea of the techniques is based on the fact that temperature generally produces global increases or decreases in structural responses that can be linearly correlated, while structural damages can cause abrupt variations near the damage locations that can be localised by suitable damage features [30-32]. It is therefore essential for the damage features to have clear damage-driven change patterns to distinguish them from those induced by temperature. The mathematical *DC* and *RDC* patterns developed in this paper can be very helpful in this situation.

In the conducted experimental validation, seven DTs were used to validate the theoretical *DC* formulas. In practice, due to economic reasons, there is a real need to keep the number of sensors at minimum. An approach that can be very useful in this circumstance is to apply Maxwell's reciprocity theorem. According to Choi *et al.* [9], using only one DT and a test-truck gradually moving and standing at the sensor-missing points will make it possible to measure the deflection of the whole bridge for damage detection purpose.

7. Conclusions

A new damage detection method was developed and presented in this paper. The method utilizes the changes in static deflections to locate and quantify the damage in Euler-Bernoulli beams through a range of the developed deflection change (*DC*) and relative deflection change (*RDC*) functions with respect to both damage location and damage severity. From the established theoretical *DC* patterns, the damage can be identified and located conveniently from a measured *DC* plot. Based on the knowledge of the damage location, the damage severity is calculated directly from the measured *RDC* through a closed-form function and the damage-severity-consistency concept. The advantages of the proposed method include: (1) it does not require an optimization algorithm or a refined FEM to locate and quantify the damage; (2) the method has a clear theoretical and physical base; and (3) the method uses the static deflection, which is one of the most reliable structural responses in structural assessment and health monitoring, especially with the recent advances in digital measurement technologies.

The feasibility and practicality of the proposed method have been verified by both numerical and experimental studies. Results from various numerical investigations showed that the proposed static damage detection method could accurately locate and quantify the damage in all single and multiple damage cases. For the experimental and the noise-added data sets, the method retains its robustness in single damage cases, and provides satisfactory results in double damage cases when the two damages are of the same extent. The proposed method can satisfactorily identify and quantify damage as minor as 10% of member stiffness reduction in noisy test environment of approximate 3.5% noise level, or even 7% noise in simulated condition.

The damage locating and quantification concepts developed and presented herein can be extended to other structures including statically determinate and indeterminate beam-type structures, and tested under real application conditions as discussed in Section 6. Research on these topics is currently underway and will be reported in future works of the present authors.

Acknowledgement

This paper is part of a study on structural health monitoring of civil structures at Queensland University of Technology (QUT), Australia. The first author greatly acknowledges financial support from the Australia Awards Scholarship program.

References

1. Chan, T. and D.P. Thambiratnam, *Structural health monitoring in Australia*. 2011, New York: Nova Science Publishers.
2. Doebling, S.W., C.R. Farrar, and M.B. Prime, *A summary review of vibration-based damage identification methods.* Shock and vibration digest, 1998. **30**(2): p. 91-105.
3. Sohn, H., C.R. Farrar, F.M. Hemez, D.D. Shunk, D.W. Stinemates, B.R. Nadler, and J.J. Czarnecki, *A review of structural health monitoring literature: 1996-2001*. 2004: Los Alamos National Laboratory Los Alamos, NM.
4. Fan, W. and P. Qiao, *Vibration-based damage identification methods: a review and comparative study.* Structural Health Monitoring, 2011. **10**(1): p. 83-111.
5. Moughty, J.J. and J.R. Casas, *A state of the art review of modal-based damage detection in bridges: Development, challenges, and solutions.* Applied Sciences, 2017. **7**(5): p. 510.
6. Pan, B., L. Tian, and X. Song, *Real-time, non-contact and targetless measurement of vertical deflection of bridges using off-axis digital image correlation.* NDT & E International, 2016. **79**: p. 73-80.
7. Feng, D. and M.Q. Feng, *Experimental validation of cost-effective vision-based structural health monitoring.* Mechanical Systems and Signal Processing, 2017. **88**: p. 199-211.
8. Tian, L. and B. Pan, *Remote bridge deflection measurement using an advanced video deflectometer and actively illuminated led targets.* Sensors, 2016. **16**(9): p. 1344.
9. Choi, I.-Y., J.S. Lee, E. Choi, and H.-N. Cho, *Development of elastic damage load theorem for damage detection in a statically determinate beam.* Computers & Structures, 2004. **82**(29): p. 2483-2492.
10. Aktan, A., K. Lee, C. Chuntavan, and T. Aksel. *Modal testing for structural identification and condition assessment of constructed facilities*. in *Proceedings-Spie the International Society for Optical Engineering*. 1994.
11. Sung, S., K. Koo, H. Jung, and H. Jung, *Damage-induced deflection approach for damage localization and quantification of shear buildings: validation on a full-scale shear building.* Smart Materials and Structures, 2012. **21**(11): p. 115013.
12. Sanayei, M. and O. Onipede, *Damage assessment of structures using static test data.* AIAA journal, 1991. **29**(7): p. 1174-1179.
13. Banan, M.R., M.R. Banan, and K.D. Hjelmstad, *Parameter estimation of structures from static response. II: Numerical simulation studies.* Journal of structural engineering, 1994. **120**(11): p. 3259-3283.

14. Banan, M.R., M.R. Banan, and K.D. Hjelmstad, *Parameter Estimation of Structures from Static Response. I. Computational Aspects.* Journal of Structural Engineering, 1994. **120**(11): p. 3243-3258.
15. Hjelmstad, K.D. and S. Shin, *Damage detection and assessment of structures from static response.* Journal of engineering mechanics, 1997. **123**(6): p. 568-576.
16. Sanayei, M., G.R. Imbaro, J.A. McClain, and L.C. Brown, *Structural model updating using experimental static measurements.* Journal of structural engineering, 1997. **123**(6): p. 792-798.
17. Wang, X., N. Hu, H. Fukunaga, and Z. Yao, *Structural damage identification using static test data and changes in frequencies.* Engineering structures, 2001. **23**(6): p. 610-621.
18. Bakhtiari-Nejad, F., A. Rahai, and A. Esfandiari, *A structural damage detection method using static noisy data.* Engineering structures, 2005. **27**(12): p. 1784-1793.
19. Chen, X.-z., Z. Hong-ping, and C. Chuan-yao, *Structural damage identification using test static data based on grey system theory.* Journal of Zhejiang University-SCIENCE A, 2005. **6**(8): p. 790-796.
20. Yang, Q. and B. Sun, *Structural damage localization and quantification using static test data.* Structural health monitoring, 2011. **10**(4): p. 381-389.
21. Kourehli, S.S., A. Bagheri, G.G. Amiri, and M. Ghafory-Ashtiany, *Structural damage detection using incomplete modal data and incomplete static response.* KSCE journal of civil engineering, 2013. **17**(1): p. 216.
22. Abdo, M.A.-B., *Parametric study of using only static response in structural damage detection.* Engineering Structures, 2012. **34**: p. 124-131.
23. Seyedpoor, S. and O. Yazdanpanah, *An efficient indicator for structural damage localization using the change of strain energy based on static noisy data.* Applied Mathematical Modelling, 2014. **38**(9): p. 2661-2672.
24. Grandić, I.Š. and D. Grandić, *Estimation of damage severity using sparse static measurement.* Journal of Civil Engineering and Management, 2017. **23**(2): p. 213-221.
25. Koo, K., S. Sung, J. Park, and H. Jung, *Damage detection of shear buildings using deflections obtained by modal flexibility.* Smart Materials and Structures, 2010. **19**(11): p. 115026.
26. Sinha, J.K., M. Friswell, and S. Edwards, *Simplified models for the location of cracks in beam structures using measured vibration data.* Journal of Sound and vibration, 2002. **251**(1): p. 13-38.
27. Ghali, A., A. Neville, and T.G. Brown, *Structural analysis: a unified classical and matrix approach*. 2014: Crc Press.
28. National Instruments. *NI 9237 Operating instructions and specifications*. 2015; Available from: http://www.ni.com/pdf/manuals/374186a_02.pdf.
29. Sohn, H., C.R. Farrar, F.M. Hemez, D.D. Shunk, D.W. Stinemates, B.R. Nadler, and J.J. Czarnecki, *A Review of Structural Health Monitoring Literature: 1996 - 2001*. Structural Control and Health Monitoring. 2001: Los Alamos, NM: Los Alamos National Laboratory.
30. Koo, K.Y., J.J. Lee, and C.-B. Yun, *Damage Detection of Bridge Structures Using Modal Flexibility under Temperature Variations.* IFAC Proceedings Volumes, 2008. **41**(2): p. 15762-15767.
31. Peeters, B. and G. De Roeck, *One‐year monitoring of the Z24‐Bridge: environmental effects versus damage events.* Earthquake engineering & structural dynamics, 2001. **30**(2): p. 149-171.
32. Kim, J.-T., J.-H. Park, and B.-J. Lee, *Vibration-based damage monitoring in model plate-girder bridges under uncertain temperature conditions.* Engineering Structures, 2007. **29**(7): p. 1354-1365.

Appendix

An analogous procedure as presented for SS beam in the theory section can be adopted for cantilever beams under a unit point load acting at the tip. The damage locating concept is illustrated in Fig. A-1a. It shows that the damage causes no changes in the beam deflection in the undamaged region from the fixed end to $x=a$. From this point onward, the *DC* increases by a third-order function with respect to x in the damaged region $a< x \leq a+b$ before linearly increases in the undamaged region $x>a+b$. The damage is therefore identified at the abrupt change between the two linear portions of the measured *DC* plot. This damage locating concept is supported from the following theoretical *DC* functions:

$$DC(x)=\begin{cases} 0 & , \quad x \leq a \\ \beta\dfrac{(x-a)^2}{6EI}(3L-2a-x), & a \leq x \leq a+b \\ \beta\dfrac{1}{6EI}\big(A+B(x-a-b)\big), & a+b \leq x \leq L \end{cases} \tag{A-1}$$

where, the damage severity derivative β is defined as in Eq. (5), while the scalars A and B are defined as:

$$A=b^2(3L-3a-b); \qquad B=3b(2L-2a-b) \tag{A-2}$$

To quantify the located damage, the *DSC* function is calculated from (10) for $x>a+b$, with a notice that the referenced $RDC^{50\%}$ function is given by Eq. (A-3). Finally, the damage severity is estimated following Eqs.

(11) and (12).

$$RDC^{50\%}(x) = \begin{cases} 0 & , \quad x \le a \\ \dfrac{(x-a)^2(3L-2a-x)}{x^2(3L-x)} & , \quad a \le x \le a+b \\ \dfrac{A+B(x-a-b)}{x^2(3L-x)} & , \quad a+b \le x \le L \end{cases} \tag{A-3}$$

For the double damage cases, the damage locating concept is illustrated in Fig. A-1b, and the damage severities can be estimated in an analogous procedure as presented for SS beam.

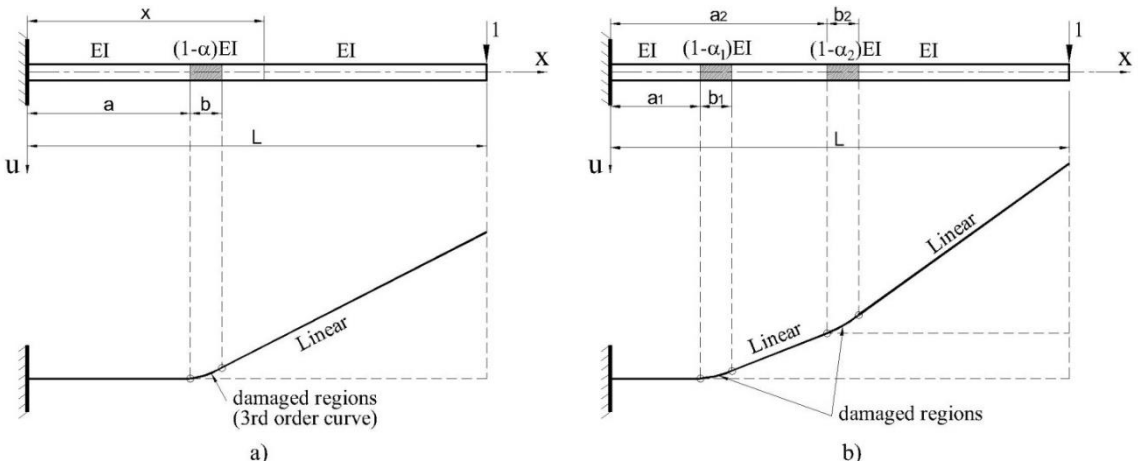

Fig. A-1. Damage locating concept of cantilever beams from *DC* plots: (a) Single damage, (b) Double damage